Bulletin of Mathematical Biology (2020) 82:4
https://doi.org/10.1007/s11538-019-00682-1

Society for Mathematical Biology

ORIGINAL ARTICLE

Predicting Pattern Formation in Multilayer Networks

Sean M. Hayes[1] · **Kurt E. Anderson**[1]

Received: 28 April 2019 / Accepted: 2 December 2019 / Published online: 20 December 2019

Abstract
We investigate how the structure of interactions between coupled oscillators influences the formation of asynchronous patterns in a multilayer network by formulating a simple, general multilayer oscillator model. We demonstrate the analysis of this model in three-oscillator systems, illustrating the role of interactions among oscillators in sustaining differences in both the phase and amplitude of oscillations leading to the formation of asynchronous patterns. Finally, we demonstrate the generalizability of our model's predictions through comparison with a more realistic multilayer model. Overall, our model provides a useful approach for predicting the types of asynchronous patterns that multilayer networks of coupled oscillators which cannot be achieved by the existing methods which focus on characterizing the synchronous state.

Keywords Synchronization · Multilayer networks · Coupled oscillators

1 Introduction

The synchronization dynamics of systems of coupled oscillators play a central role in a tremendous range of phenomena across the physical, biological, and social sciences (Faloutsos et al. 1999; Freeman 1996; Holland and Hastings 2008; Jeong et al. 2000; Varela et al. 2001). A system of coupled oscillators can represent any dynamical system characterized by interactions between components with regular fluctuations in its state variables such as neurons, heart cells, animal populations, and power generators. Determining how and why oscillators in these systems either converge on the same set of dynamics (synchrony) or differentiate from one another (asynchrony) is central to both understanding and managing these types of systems (Albert and Barabási 2002; Boccaletti et al. 2006; Strogatz 2001).

A valuable tool for investigating the synchronization dynamics of coupled oscillator systems has been the Kuramoto model, which features extremely simple and general-

✉ Sean M. Hayes
seanmhayes89@gmail.com

[1] Department of Evolution, Ecology, and Organismal Biology, University of California Riverside, Riverside, CA 92521, USA

izable oscillator dynamics describing constant phase evolution following a sine wave and diffusion-based coupling between oscillators (Kuramoto 1975; Strogatz 2000). However, due to the simplicity of the model the coupling of Kuramoto oscillators is only able to influence phase, while in many systems coupling also influences the internal dynamics of oscillators. Specifically, in multilayer networks where oscillations are produced by the interactions between multiple types of internal components, the coupling of like components between oscillators can cause differences in not only phase but also the amplitude of the oscillatory equilibrium. Thus, the study of multilayer networks can reveal much about the role of structure in the synchronization dynamics in more complex real-world systems (Boccaletti et al. 2014).

Unsurprisingly, the synchronization dynamics of both single- and multilayer oscillatory systems can be extremely complex. In the simplest case where every oscillator and their internal components are identical, total synchronization is expected and intuitive. However, even when oscillators are identical, these systems are able to differentiate into a variety of dynamical regimes, reaching stable asynchronous equilibria: a phenomenon known as pattern formation (Cross and Hohenberg 1993; Turing 1952). These patterns are primarily known to be caused by Turing instabilities, wherein the synchronized, homogeneous state is destabilized by coupling between the components of the system (Turing 1952). It is not necessary for the synchronous state to be destabilized however; coupling among oscillators can also stabilize a variety of alternative asynchronous equilibria that coexist with the synchronous state (Nakao and Mikhailov 2010; Wolfrum 2012). In this case, the equilibrium found by the system depends on initial conditions and may shift with large enough perturbations depending on the landscape of equilibria and their attractive properties.

Despite the appearance of stable asynchronous equilibria even in the absence of Turing instability, pattern formation has been studied primarily by characterizing the stability of the synchronous state. Specifically, the master stability function (MSF) formalism is commonly used to determine the conditions for stable synchrony in a given system and the general ability of individual structures to maintain synchrony (Arenas et al. 2008; Barahona and Pecora 2002; Pecora and Carroll 1998). This approach considers the local stability of the synchronized equilibrium, particularly whether the system will return to synchrony following a small asynchronous perturbation. This tells us nothing about the number and qualities of asynchronous equilibria, however, as it considers a system's behavior only near the synchronous equilibrium. Studies on pattern formation in multilayer networks in particular have, so far, focused on the MSF and similar methods (Asllani et al. 2014; Brechtel et al. 2018; Hata et al. 2014; Kouvaris et al. 2015) for characterizing the stability of the synchronized state. Thus, it is necessary to develop alternative approaches to further investigate the role of structure in the formation and stabilization of alternative asynchronous equilibria, particularly in multilayer networks.

Some approaches have been effective in illuminating the role of structure in the formation of asynchronous patterns, particularly by analyzing the spectral properties of the network's adjacency matrix. One approach demonstrates that for an asynchronous pattern to be stable, the 'coloring' of oscillators (where oscillators with the same color are synchronized) must be balanced such that all oscillators of the same color are connected to the same numbers and colors of other oscillators (Stewart et al. 2003).

A variety of methods for determining all the balanced colorings from a given structure have been developed (Aguiar and Dias 2014; Kamei and Cock 2013). From a balanced coloring, a 'quotient network' can be constructed, which reduces the network to interactions between differently colored nodes (Stewart et al. 2003). Another approach identifies the special case where eigenvectors are localized to specific subgraphs within the network (Do et al. 2012). The authors demonstrate that in this case the relationship between dynamics and topology can be understood within subgraphs independent of the network in which they are embedded and that this analysis can aid in understanding and control of any network containing such subgraphs, or to which such a subgraph could be added. While these approaches reveal much about how structure constrains asynchronous patterns, predicting how the dynamics of oscillators change due to asynchrony in the general case remains an unsolved problem.

To move beyond the focus on the stability of the synchronized state and investigate the effect of interaction structure on both the conditions for and dynamics of alternative asynchronous equilibria, we develop and analyze a simple multilayer oscillator network model. We illustrate the use of this model in predicting the emergence and effect of asynchronous patterns on oscillator phase and amplitude by first analyzing the structure of three-oscillator networks. These systems are small enough to be solved effectively, while complex enough to provide insight into the mechanisms underlying pattern formation in more complex structures. Through this analysis, we discuss how each oscillator's potential for differentiation is determined by its position within a network structure and the mechanisms underlying the differentiation of oscillator dynamics.

Finally, we compare the predictions of our model with the numerical results of a more complex multilayer model characterized by oscillations generated via nonlinear interactions among oscillator components. Our model successfully predicts many of the patterns generated by this more complex model, despite being significantly simpler. Overall, our model provides a useful starting point for the analysis of pattern formation in multilayer networks which generalizes readily to more complex and realistic systems.

2 Multilayer Oscillator Network Model

Our multilayer oscillator network model is:

$$x_i' = \delta \sum_{j=1} L_{ij} r_j \cos(\theta_j - \theta_i) + \psi(1 - r_i) \tag{1}$$

$$y_i' = \delta \sum_{j=1} L_{ij} r_j \sin(\theta_j - \theta_i) \tag{2}$$

$$\theta_i' = \omega + \tan^{-1}\left(\frac{y_i'}{x_i'}\right) \tag{3}$$

$$r_i' = \sqrt{(r_i - x_i')^2 + y_i'^2} - r_i \tag{4}$$

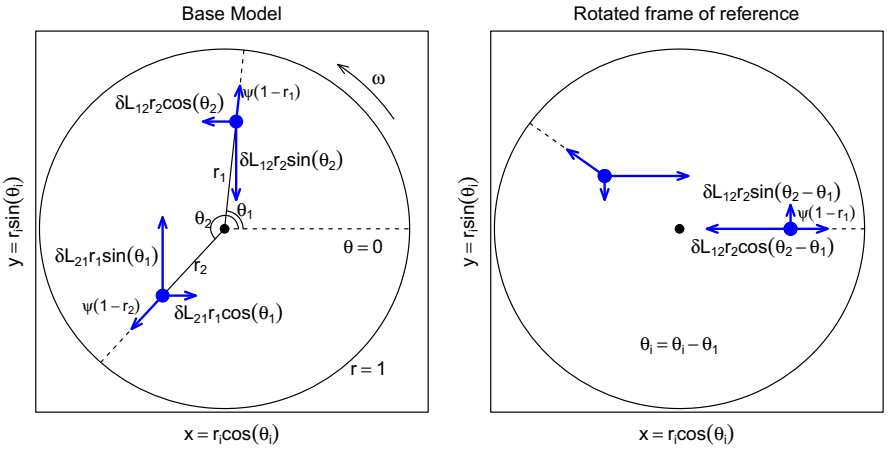

Fig. 1 Illustration of the components of our multilayer oscillator network model. Each oscillator i is pulled toward the state of its neighbors j based on coupling strength δ and interaction strength L_{ji}, with the x and y dimensions acting as independent layers. Oscillators are also repelled from the center toward the intrinsic limit cycle based on the strength of repulsion ψ and distance from the intrinsic limit cycle $(1-r_i)$. Calculations for the net effect of these forces on each oscillator i are simplified by rotating the frame of reference by oscillator i's phase such that the phase of all oscillators j, $\theta_j = \theta_j - \theta_i$, making $\theta_i = 0$, $y_i = 0$, and $x_i = r_i$ (Color figure online)

We illustrate the components of our model in Fig. 1. Our model is constructed similarly to the Kuramoto model (Kuramoto 1975), where θ_i is the phase of oscillator i and r_i its amplitude. Internally, each oscillator undergoes constant phase evolution ω around a limit cycle described by the unit circle, where the x dimension is $\cos(\theta)$ the y dimension is $\sin(\theta)$. Oscillators are coupled independently on both the x and y dimensions by the matrix L with coupling strength δ, such that δL_{ij} describes the effect of coupling from oscillator j on oscillator i. The matrix L is the negative Laplacian, or $A-D$ where A is the adjacency matrix and D is the diagonal degree matrix. Thus, off-diagonal elements of L are positive while each diagonal element L_{ii} is the negative sum of the off-diagonal elements of row i.

Because oscillators are coupled on both the x and y dimensions, amplitude r can vary, unlike the Kuramoto model. This allows oscillators to escape their intrinsic limit cycle ($r = 1$). To simulate the behavior of real limit cycles with unstable fixed points at their center, we introduce the parameter ψ for the repelling force of the center; the term $\psi(1 - r_i)$ causes amplitude r to move toward the limit cycle $r = 1$ at a fraction of ψ proportional to the oscillator's distance from the original limit cycle.

Calculations are simplified by rotating the frame of reference about the limit cycle by θ_i such that the phase of all oscillators j becomes $\theta_j = \theta_j - \theta_i$, making $\theta_i = 0$, $y_i = 0$, and $x_i = r$, as illustrated in Fig. 1. It should be noted that this rotation assumes that coupling strength δ and interaction structure L are same for both the x and y dimensions of the oscillators. In our formulation of this model, this holds true; however, it is possible to alter the model such that interactions among oscillators differ between the x and y dimensions as they may for many multilayer systems. Additionally, the changes in x and y dimensions shown in Eqs. 1 and 2 are changes

post-rotation to simplify calculation of the change in phase and amplitude and thus do not represent the actual change in the x and y dimensions of each oscillator. Finally, as ω is constant (all oscillators are identical), we set $\omega = 0$ so that the only changes in phase analyzed are those relative to the phase of other oscillators and not intrinsic rotation about the limit cycle.

From Eq. 3, we observe that the phase of oscillator i relative to the other oscillators is locked only if $y_i' = 0$, or:

$$\theta_i = \tan^{-1}\left(\frac{\sum_{j\neq i} L_{ij} r_j \sin(\theta_j)}{\sum_{j\neq i} L_{ij} r_j \cos(\theta_j)}\right) \tag{5}$$

This condition can be satisfied regardless of each oscillator's amplitude r_j or the strength of interactions L_{ij} if $\sin(\theta_j - \theta_i) = 0$ for all j, meaning $\theta_i = \theta_j \pm n\pi,\ n \in \mathbb{N}$ for all j. Alternatively, the sum of all interactions with other oscillators must balance to zero, or $\sum_{j\neq i} L_{ij} r_j \sin(\theta_j - \theta_i) = 0$.

From Eq. 4, amplitude is locked when phase is locked ($y_i' = 0$) and $x_i = 0$, or:

$$r_i = \frac{\frac{\psi}{\delta} + \sum_{j\neq i} L_{ij} r_j \cos(\theta_j - \theta_i)}{\frac{\psi}{\delta} - L_{ii}} \tag{6}$$

With these conditions together, we can identify all equilibria present in a given system, including the trivial case of total synchrony ($\theta_i = 0$ and $r_i = 1$ for all i).

3 Three-Oscillator Systems: Equilibrium Phases

To demonstrate the analysis of our model and shed light on the effects of structure on pattern formation, we analyze the effects of structure L on the equilibria of systems of three oscillators. There are two possible structures which connect all three oscillators. The first is a triangle where every oscillator is connected to the other two, and the second is a line where two outer oscillators connect to a single middle oscillator. When describing phases, we rotate our point of reference about the unit circle such that the phase of each oscillator is described by their difference from the first oscillator, $\theta_i - \theta_1$. The first oscillator thus serves as our point of reference and is always 0 ($\theta_1 - \theta_1$). This simplifies analysis and highlights the differences between oscillator phases as the meaningful driver of dynamics.

As discussed, the condition for phase locking (Eq. 5) has a guaranteed solution independent of each oscillator's amplitude or the strength of interactions when $\sin(\theta_j - \theta_i) = 0$ for all i, j, or $\theta_i = \theta_j \pm n\pi,\ n \in \mathbb{N}$. As the period of each oscillator is 2π, π and $-\pi$ are equivalent and we have two possible phases for each oscillator: equal ($\theta_i - \theta_1 = 0$) or antiphase ($\theta_i - \theta_1 = \pm\pi$) to the first oscillator. This gives us three sets of asynchronous equilibrium phases for each structure, each with two oscillators sharing a phase and one antiphase to them. The amplitude of these oscillators can then be determined separately as we describe later.

Phases can also be locked when the effects of other oscillators on phase are balanced and cancel out; $L_{ij}r_j \sin(\theta_j - \theta_i) = -L_{ik}r_k \sin(\theta_k - \theta_i)$. Unlike the solutions with all phases equal or antiphase, these do depend on the strength of interactions and amplitude. This type of solution also requires that each oscillator has at least two connections to balance against each other, and as a result, these equilibria are possible only for the triangle structure and not the line. We find by substitution the conditions for these equilibria:

$$L_{12}L_{23}L_{31} = L_{21}L_{32}L_{13} \tag{7}$$

$$\theta_2 - \theta_1 = \pm\cos^{-1}\left[\frac{(L_{23}L_{13}r_3)^2 - (L_{21}L_{13}r_1)^2 - (L_{12}L_{23}r_2)^2}{2(L_{21}L_{13}r_1)(L_{12}L_{23}r_2)}\right] \tag{8}$$

$$\theta_3 - \theta_1 = \mp\cos^{-1}\left[\frac{(L_{32}L_{12}r_2)^2 - (L_{31}L_{12}r_1)^2 - (L_{13}L_{32}r_3)^2}{2(L_{31}L_{12}r_1)(L_{13}L_{32}r_3)}\right] \tag{9}$$

The conditions specifying $\theta_2 - \theta_1$ and $\theta_3 - \theta_1$ turn out to be the equations for finding the angle of triangle from its sides, the law of cosines. In conjunction with a constraint on interaction structure, Eq. 7, these conditions specify that phases are locked only if the angles $\pi - (\theta_2 - \theta_1)$, $\pi - (\theta_3 - \theta_1)$, and $\pi - (\theta_3 - \theta_2)$ form a triangle with sides equal to the oscillator's amplitudes scaled by their interactions with other oscillators. The weighting of the sides of the triangle may differ between the equations for $\theta_2 - \theta_1$ and $\theta_3 - \theta_1$ as the first condition ensures that the angles of both triangles agree by requiring that all sides of the triangle for $\theta_3 - \theta_1$ are proportional to the sides of the triangle for $\theta_2 - \theta_1$ by $\frac{L_{23}}{L_{32}}$.

From these conditions, we observe that phase locking for these equilibria depends on ratios of amplitudes and interaction strengths, specifically $\frac{L_{ij}r_j}{L_{ik}r_k}$. Thus, equilibrium phase can be determined independent of amplitude if the ratios remain constant, or $r_1' = r_2' = r_3'$. To illustrate, we consider the case of a triangle with equal interactions between all oscillators ($L_{ij} = 1$ for all i, j) and equal amplitudes for all oscillators, making $\frac{L_{ij}r_j}{L_{ik}r_k} = 1$ for all i, j, k. This satisfies the constraint on structure in Eq. 7 and simplifies Eqs. 8 and 9 to $\theta_2 - \theta_1 = \pm\frac{2\pi}{3}$ and $\theta_3 - \theta_1 = \mp\frac{2\pi}{3}$. Following this, Eq. 4 simplifies to $\frac{dr_i}{dt} = \delta(-3r_i) + \psi(1 - r_i)$, making the change in amplitude equal for all oscillators if the amplitudes are equal. Thus, there is an asynchronous equilibrium at $r_1 = r_2 = r_3$ and $\theta_2 - \theta_1 = \pm\frac{2\pi}{3}$, and $\theta_3 - \theta_1 = \mp\frac{2\pi}{3}$.

From the conditions for phase locking, we find that structure plays a role in enabling the emergence of asynchronous equilibria on two levels. First, the 'qualitative' structure, or the presence/absence of interactions among oscillators, determines whether oscillators can be phase-locked without being equal or antiphase to each other. This effect immediately differentiates the line and triangle structures from one another, enabling a much wider range of possible asynchronous patterns for the triangle than for the line. Second, the 'quantitative' structure, or the strength of interactions among oscillators, provides an additional condition which must be met for equilibrium phases

that are not equal or antiphase to be possible (Eq. 7) and additionally plays a role in arbitrating the relationship between phase and amplitude in the more complex case of equilibria due to its appearance in the ratios $\frac{L_{ij}r_j}{L_{ik}r_k}$ (Eqs. 8, 9).

Overall, oscillators with more neighbors to interact with have more possibilities for differentiation. An oscillator with a single interaction must be equal in phase or antiphase with its neighbor, while an oscillator with two neighbors can also be phase-locked if the neighbor's effects cancel out. The complexity of possible pattern formation mechanisms continues to scale with the number of oscillators and interactions; an oscillator with three neighbors can be phase-locked by having one neighbor cancel the other two, by being antiphase or equal to one and having the other two cancel, and so on. As a result, the number of possible asynchronous patterns can be expected to scale with the complexity of the network.

4 Three-Oscillator Systems: Equilibrium Amplitudes

Next we consider how interaction structure L influences the amplitude of oscillators, first by analyzing the conditions for amplitude locking, found through substitution of Eq. 6:

$$r_i = \frac{\psi^3 + \psi^2\delta F(i) + \psi\delta^2 G(i)}{\psi^3 + \psi^2\delta H_1 + \psi\delta^2 H_2 + \delta^3 H_3} \tag{10}$$

where

$$\begin{aligned}
B_{ij} &= L_{ij}\cos(\theta_i - \theta_j)\\
F(i) &= (B_{ij} + B_{ik}) - (B_{jj} + B_{kk})\\
G(i) &= (B_{kj}B_{ik} + B_{ij}B_{jk} + B_{jj}B_{kk})\\
&\quad - (B_{ij}B_{kk} + B_{jj}B_{ik} + B_{jk}B_{kj})\\
H_1 &= -(B_{11} + B_{22} + B_{33})\\
H_2 &= (B_{11}B_{22} + B_{11}B_{33} + B_{22}B_{33})\\
&\quad - (B_{12}B_{21} + B_{13}B_{31} + B_{23}B_{32})\\
H_3 &= (B_{33}B_{12}B_{21} + B_{22}B_{13}B_{31} + B_{11}B_{23}B_{32})\\
&\quad - (B_{11}B_{22}B_{33} + B_{12}B_{23}B_{31} + B_{21}B_{13}B_{32}).
\end{aligned}$$

The terms of Eq. 10 are made up of combinations of elements B, a matrix combining the effect of phase differences and the matrix of interaction strengths between oscillators L. Of these terms, $F(i)$ and $G(i)$ can differ for each oscillator, while H_1, H_2, and H_3 will be constant for all oscillators in the system.

In the cases where phase is locked independently from amplitude, amplitude is straightforward to calculate using the parameters of the system. To illustrate we show examples of the calculated amplitude for each of the equilibrium phases, we identified in the previous section in Table 1, where interactions are equal among all oscillators for both structures ($L_{ij} = 1$ for all i, j). These results highlight an interesting difference

Table 1 Calculated amplitudes for selected asynchronous equilibria

$\theta_2 - \theta_1$	$\theta_3 - \theta_1$	r_1 (end)	r_2 (mid.)	r_3 (end)
Line structure				
0	$\pm\pi$	.975	.8	.775
$\pm\pi$	0	.8	.6	.8
$\pm\pi$	$\pm\pi$	.775	.8	.975
Triangle structure				
0	$\pm\pi$	.8	.8	.6
$\pm\pi$	0	.8	.6	.8
$\pm\pi$	$\pm\pi$	.6	.8	.8
$\pm 2\pi/3$	$\mp 2\pi/3$	.7	.7	.7

The parameters used were equal interaction strengths for all interactions ($L_{ij} = 1$ for all i, j), $\delta = .1$, and $\psi = .7$. For the line structure, oscillators 1 and 3 are at the ends and do not connect to each other ($L_{13} = L_{31} = 0$) while oscillator 2 is the middle connected to both. For the triangle structure each oscillator is equivalent due to equal weighting of interactions

between the line and triangle structures: for the triangle, oscillators with equal phases have the same amplitude, while oscillators at the end of the line structure (1 and 3) have differing amplitudes when phase is equal to the middle oscillator. Thus, despite oscillators in the line structure being constrained to two phases, all three are able to differentiate and avoid total synchronization with their neighbors.

We can determine the conditions for oscillators with equal phase to exhibit different amplitudes by determining whether $F(i) = F(j)$ and $G(i) = G(j)$ in Eq. 10. In particular, for two oscillators to maintain different amplitudes while sharing the same phase, at least one of these conditions must be false:

$$\begin{aligned} F(i) = F(j) &\leftrightarrow (B_{ij} + B_{ik}) - (B_{ji} + B_{jk}) = 0 \\ G(i) = G(j) &\leftrightarrow B_{ik}[(B_{ki} + B_{kj}) - (B_{ji} + B_{jj})] \\ &\quad + B_{jk}[(B_{ii} + B_{ij}) - (B_{ki} + B_{kj})] \\ &\quad + B_{kk}[(B_{ji} + B_{jj}) - (B_{ii} + B_{ij})] = 0 \end{aligned}$$

These conditions will always be true if the set of interactions both to and from the two oscillators i and j are isomorphic, or $B_{i.} \cong B_{j.} \rightarrow F(i) = F(j)$, $B_{.i} \cong B_{.j} \rightarrow G(i) = G(j)$. As we observed, when interactions are equal among all oscillators ($L_{ij} = 1$ for all i, j), all oscillators are isomorphic in the triangle structure and thus will have the same amplitude if phase is equal. For the line structure, the two ends are isomorphic while the center is not, and so as we observed the ends will share the same amplitude if their phase is equal while the amplitude of the ends will differ from the middle when phase is equal.

From this, the symmetry of an interactions structure, which is defined by the automorphisms of the interaction structure, is shown to play a significant role in constraining the types of asynchronous patterns possible. The ability to maintain differences in dynamics among oscillators with the same phase through variation in

amplitude can create a variety of patterns unique to multilayer networks; however, this is not possible between oscillators which are isomorphic. As a result, the addition or removal of links which increase the symmetry of an interaction structure prevents the formation of certain patterns, as observed in our comparison between the line and triangle structures. Overall, structures with low self-symmetry but a high degree of connectance among oscillators are expected to foster the greatest number of possible asynchronous patterns.

By further analyzing Eq. 10, we can identify the specific elements of structure that drive of differences in amplitude between oscillators. First, we observe that the terms of this equation correspond to important subcomponents of the matrix B, where $B_{ij} = L_{ij}\cos(\theta_i - \theta_j)$, specifically the determinant $\det(B)$ trace, $\mathrm{tr}(B) = \sum B_{ii}$ and cofactors $C_{ij} = (-1)^{i+j}\det(D_{ij})$, where D_{ij} is a submatrix of B with row i and column j removed:

$$
\begin{aligned}
F(i) &= \sum_{j=1}(B_{ij}) - \mathrm{tr}(B) \\
G(i) &= \sum_{j=1} C_{ji} \\
H_1 &= -\mathrm{tr}(B) \\
H_2 &= \sum_{j=1} C_{jj} \\
H_3 &= -\det(B)
\end{aligned}
$$

As $L_{ii} = -\sum_{j\neq i} L_{ji}$, the sum of all columns of L equals 0. Therefore, when all phases are equal $L = B$, making $F(i) = H_1$, $G(i) = H_2$, and $H_3 = 0$, thus $r = 1$ for all oscillators. This corresponds to our case of total synchrony with no deviation in amplitude from the original limit cycle.

The conditions which maximize change in amplitude from the basal state $r = 1$ can be found by minimizing $F(i)$ and $G(i)$ and maximizing H_1, H_2, and H_3. $F(i)$ and H_1 both depend on the negative sum of the diagonal elements of the coupling matrix L, which is the total of all interaction strengths in the system. High total interaction strengths increase both H_1 and $F(i)$; however, $F(i)$ is not affected by the value of L_{ii}. $F(i)$ can also be reduced independently from H_1 by phase differences greater than $\pi/2$ and less than $3\pi/2$ between oscillator i and its neighbors, which make the elements B_{ij} negative. $F(i)$ is minimized for a given interaction matrix when oscillator i is antiphase with its neighbors, as in the two-cluster solutions of Table 1. $F(i)$ is then further reduced the greater the strength of interaction with antiphase neighbors.

Next, $G(i)$ and H_2 depend on the cofactors of B. For H_2, the cofactors are the determinants of the matrices describing the coupling between each pair of oscillators. For cofactor i, i this value is

$$
C_{ii} = (L_{jj}L_{kk}) - (L_{jk}L_{kj})\cos^2(\theta_j - \theta_k). \tag{11}
$$

The maximum for each of these values is $L_{jj}L_{kk}$, which is realized either when L_{jk} and/or L_{kj} is zero or when $\theta_j - \theta_k = \pi/2 \pm n\pi,\ n \in \mathbb{N}$. In cases where all oscillators are equal or antiphase, this simplifies to $(L_{jj}L_{kk}) - (L_{jk}L_{kj})$ as $\cos^2(\pi) = \cos^2(0) = 1$. Substituting $L_{ii} = -\sum_{j \neq i} L_{ij}$, cofactor i, i becomes $L_{ji}L_{ki} + L_{ji}L_{kj} + L_{jk}L_{ki}$, illustrating the dependence of these values on interactions with the third oscillator, i. In cases where the phases of oscillators are locked by balancing their interactions, each cofactor is increased the closer $\theta_j - \theta_k$ is to $\pi/2 \pm n\pi,\ n \in \mathbb{N}$, which also corresponds to an increasing effect of oscillators j and k on the other's phase, requiring an equally strong opposing effect for phase to be locked. Overall, H_2 is increased by balanced interactions among oscillators.

The cofactors determining $G(i)$ include one of the cofactors from H_2, C_{ii}, the determinant of the coupling matrix between j and k. $G(i)$ also includes the signed determinants of the other submatrices constructed from L with column i removed. Cofactor j, i is

$$\begin{aligned} C_{ji} = {} & L_{ij}L_{jk}\cos(\theta_i - \theta_j)\cos(\theta_j - \theta_k) \\ & - L_{jj}L_{ik}\cos(\theta_i - \theta_k). \end{aligned} \tag{12}$$

The minimum for these cofactors is $-(L_{ji}L_{ik} + L_{jk}L_{ik} + L_{ij}L_{jk})$, as $L_{jj} = -\sum_{i \neq j} L_{ij}$. This occurs for a given interaction matrix when i is antiphase with both j and k, or $\theta_i - \theta_j$ and $\theta_i - \theta_k$ equals $\pi \pm n2\pi,\ n \in \mathbb{N}$, and $\theta_j - \theta_k$ equals zero. Both C_{ji} and C_{ki} are minimized by these phase differences. These conditions are similar to those that minimize $F(i)$; however, $G(i)$ is also minimized by strong interactions between its two neighbors, L_{jk} and L_{kj}, and high total interaction strength for each, L_{jj} and L_{kk}.

Finally, H_3 is the negative determinant of B. This value expands to

$$\begin{aligned} -\det(B) = {} & L_{ij}L_{ji}(L_{ki} + L_{kj})(1 - \cos^2(\theta_i - \theta_j)) \\ & + L_{ik}L_{ki}(L_{ji} + L_{jk})(1 - \cos^2(\theta_i - \theta_k)) \\ & + L_{jk}L_{kj}(L_{ij} + L_{ik})(1 - \cos^2(\theta_j - \theta_k)) \\ & + (L_{ij}L_{jk}L_{ki} + L_{ik}L_{kj}L_{ji})(1 - \cos(\theta_i - \theta_j) \\ & \times \cos(\theta_i - \theta_k)\cos(\theta_j - \theta_k)). \end{aligned} \tag{13}$$

Maximizing H_3 depends on the specific interaction matrix, as no one set of phase differences can maximize $1 - \cos^2(\theta_i - \theta_j)$ for all i, j. In the case where all interaction strengths are equal, $L_{ij} = 1$ for all i, j, H_3 is maximized when $\theta_j - \theta_i = \pm 2\pi/3$ and $\theta_k - \theta_i = \mp 2\pi/3$, the triangle's three-cluster equilibrium in Table 1. In this case, H_3 like H_2 is increased by even phase differences among oscillators due to the evenly distributed interaction strengths between oscillators. In other cases, the maximum for H_3 will shift such that oscillators with stronger interactions $(L_{ij}L_{ji})$ should have phase differences closer to $\pi/2 \pm n\pi,\ n \in \mathbb{N}$, making $\cos^2(\theta_i - \theta_j)$ closer to zero and indicating a stronger effect of i and j on each other's phase.

Altogether, these conditions provide insight into the mechanisms by which interaction structure changes oscillator dynamics. System-wide reductions in amplitude

are promoted by high total interaction strengths (H_1), evenly distributed interactions among oscillators (H_2), and phase differences which match the pattern of interactions among oscillators (H_3). Curiously, both high total interaction strength and even distribution of interaction strengths are both known to promote synchrony (Arenas et al. 2008; Watts and Strogatz 1998). This may not be surprising, as the conditions which maximize differences in amplitude also suggest strong effects of oscillators on one another which promotes synchronization. This presents an interesting trade-off in maximizing either the frequency of asynchrony, in terms of the range of initial conditions which will lead to asynchrony, versus the strength of the effect of asynchrony on oscillator amplitude.

In addition to the aforementioned system-wide effects, $F(i)$ and $G(i)$ describe the conditions which influence the amplitudes of individual oscillators. Specifically, oscillator i's amplitude is reduced by strong interactions with neighbors j and k when both have high phase differences with i. Additionally, strong interactions and low phase differences between j and k reduce i's amplitude. These effects compete with the system-wide effects on amplitude: the conditions which minimize $F(i)$ and $G(i)$ have all oscillators are equal or antiphase, constraining H_3 to zero and limiting H_2. The ultimate effect of each of these terms on amplitude depends on the center resistance ψ and coupling strength δ. Higher values of coupling strength δ increase the effect of H_3 in particular and the effect of $G(i)$ and H_2 relative to $F(i)$ and H_1, respectively. Higher values of center resistance ψ have the opposite effect, having no effect on H_3 while increasing $F(i)$ and H_1 relative to $G(i)$ and H_2.

5 Simulation Results and Comparison with Ecological Model

We compare the dynamics of our model with a commonly studied and more complex ecological model, the Rosenzweig–MacArthur predator–prey model (Rosenzweig and MacArthur 1963). This model has been used previously to study the effects of structure on dynamics (Holland and Hastings 2008; Hayes and Anderson 2018), though analytical prediction from the model has been challenging due to its complexity. Other work has been successful in extracting analytical predictions of the conditions for and qualities of synchronous and asynchronous states from this model (Goldwyn and Hastings 2008), but only when coupling is too weak to change the amplitude of limit cycles, only the phase of oscillations. By contrast, we show that our model can reproduce much of the behavior of the more complicated Rosenzweig–MacArthur model while still being accessible to direct analytical prediction even in the case of strong coupling.

Specifically, we compare our model with the non-dimensional form of the Rosenzweig–MacArthur model with dispersal between subpopulations of predators and prey, which has previously been used to study the effects of structure on dynamics (Holland and Hastings 2008; Goldwyn and Hastings 2008; Hayes and Anderson 2018):

$$h_i' = h_i(1 - h_i K) - \frac{p_i h_i}{1 + h_i} + \delta \sum_{j=1}^{n} L_{ij} h_j \tag{14}$$

$$p_i' = \frac{ep_i h_i}{1 + h_i} - mp_i + \delta \sum_{j=1}^{n} L_{ij} p_j \tag{15}$$

where h_i and p_i are the abundance of prey and predators, respectively, in subpopulation i, K represents prey self-regulation, e the intensity of predation, and m predator mortality. L is the structure of movement among subpopulations and δ the rate of movement, both of which are equivalent to the structure L and strength δ of coupling among oscillators in our model. In comparing the two models, each subpopulation of predator and prey are equivalent to the x and y dimensions of an oscillator. The limit cycle of the predators and prey is centered around the system's unstable fixed point, $\hat{h} = m(e - m)$ and $\hat{p} = (1 + \hat{h})(1 - \hat{h}K)$.

Between the two models, interactions between oscillators are the same while each differs in terms of the local dynamics generating oscillations. While the simple limit cycle followed by our general multilayer model is explicitly constructed, the Rosenzweig–MacArthur model's limit cycle is an emergent property of nonlinear interaction between the predator and prey, specifically $(p_i h_i)/(1+h_i)$. Thus, our comparison is intended to illustrate the degree to which interactions in oscillators alone can be used to predict the emergence of asynchronous states which generalize across different types of local dynamics.

We compare the asynchronous states exhibited and dynamics produced by both models in Fig. 2. We use parameters for the ecological model used in previous work (Holland and Hastings 2008; Hayes and Anderson 2018) to represent systems with strong density dependence in prey and high predation, creating high amplitude oscillations which emphasize the role of spatial structure in these systems. Despite the different shape of limit cycle and intrinsic nonlinearity of the ecological model, the asynchronous states it produces and their dynamics resemble those found in our multilayer oscillator model. In particular, the pattern of phases and amplitudes of the two-cluster and three-cluster triangle equilibria are very similar, demonstrating similar mechanisms underlying the formation of asynchronous equilibria in both models. Specifically, we observe the action of both the phase locking of antiphase oscillators (Fig. 2 two cluster) and the balancing of phase differences to produce asynchronous equilibria (Fig. 2 three-cluster triangle) in the Rosenzweig–MacArthur predator–prey model.

By contrast, we note substantial differences in the equilibria produced by the multilayer oscillator and Rosenzweig–MacArthur for the three-cluster line treatment. While the Rosenzweig–MacArthur model is asynchronous in this case, the amplitudes of each oscillator do not follow the expected pattern and differences in phase are irregular. Irregularity in phase difference occurs due to differences in the period of each oscillator's limit cycle, a feature of the Rosenzweig–MacArthur model not accounted for in our model. In the multilayer oscillator model, the phase evolution of each oscillator is fixed and equal (ω), locking each oscillator to the same period of fluctuations regardless of any other details about the state of the system. In the Rosenzweig–MacArthur model, oscillations depend on the nonlinear interaction between prey h_i and predators p_i, leading to a great deal of potential variation in period. We illustrate this variation in Table 2 by summarizing the periods of oscillations observed in each equilibria for the

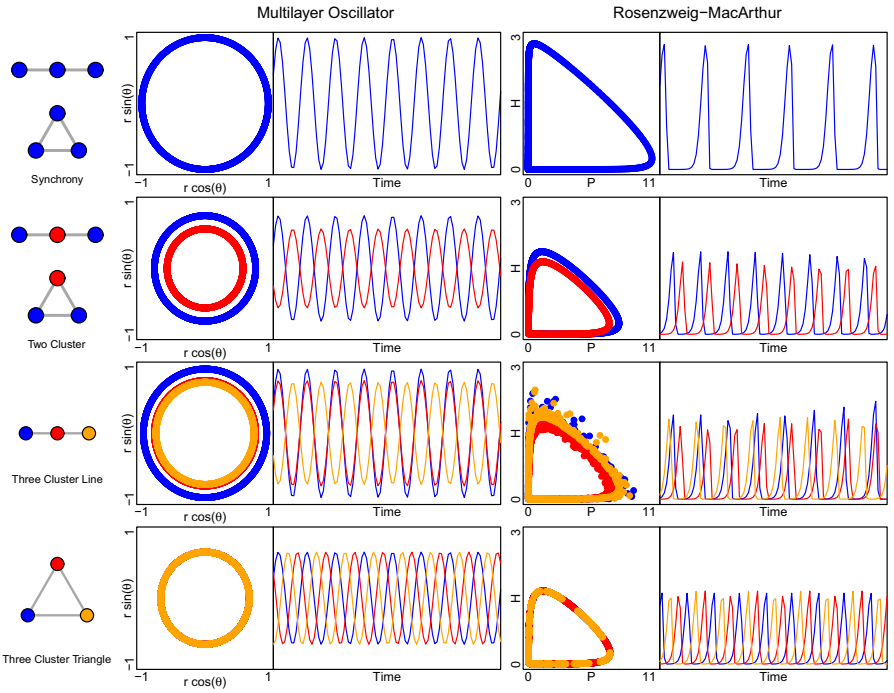

Fig. 2 Comparison between the asynchronous states observed in the Rosenzweig–MacArthur model and our multilayer oscillator model. Simulations were run until dynamics were stationary for 5000 timesteps. We used the parameters $\omega = .5$, $\delta = .1$, and $\psi = .7$ for the multilayer model and $K = .3$, $e = 5$, $m = 1$, and $\delta = .001$ for the Rosenzweig–MacArthur model following (Holland and Hastings 2008; Hayes and Anderson 2018). The two three-oscillator interaction structures were used, a line and a triangle, both with $L_{ij} = 1$ for all i, j. Initial conditions known to produce asynchrony in the multilayer model were used, with $r = 1$ and $\theta = [0, 0, 0]$ for synchrony, $[0, \pi, 0]$ for two clusters, $[0, 0, \pi]$ for three clusters on the line, and $[0, 2\pi/3, -2\pi/3]$ for three clusters on the triangle. For the Rosenzweig–MacArthur model, the same initial conditions were translated into the x and y dimensions, with amplitude rescaled and centered around the limit cycle, predator abundance $p_i = \hat{p} + r_i \cos(\theta_i) +$ and prey $h_i = \hat{h} + .25 r_i \sin(\theta_i)$ (Color figure online)

Rosenzweig–MacArthur model. In particular, we note that the period of each oscillator is same for the two-cluster and three-cluster triangle equilibria, which agree with the predictions of the multilayer oscillator model, while the period of each oscillator varies dramatically for the three-cluster line equilibrium.

While our model offers a simplified look at the effect of interaction structure between oscillators on the formation of asynchronous equilibria, many of its features can be readily generalized to more complex systems. Without modification, it successfully predicts the pattern of amplitudes and phases of several of the more complex model's equilibria. While it fails to predict the pattern of amplitudes and phases of the three-cluster line equilibrium, it is still effective at predicting the conditions which lead to asynchronous equilibria in all three tested cases. Further adjustments to the model, specifically changing the rate of phase evolution ω to depend on the cycle's amplitude or phase, could be used to capture the effect of nonlinearities on cycle

Table 2 Cycle periods for each oscillator in all equilibria observed in the Rosenzweig–MacArthur model

Equilibrium type	Oscillator	Min. period	Mean period	Max. period
Synchrony	Blue	18.33	18.49	18.66
Two cluster	Blue	12.04	12.09	12.19
	Red	12.05	12.08	12.20
Three-cluster line	Blue	12.06	12.27	13.91
	Red	11.29	12.17	12.71
	Orange	12.05	12.43	15.68
Three-cluster triangle	Blue	11.31	11.50	11.68
	Red	11.42	11.50	11.57
	Orange	11.30	11.50	11.69

Periods were calculated from the last 500 timesteps of each simulation as the difference in timing between cycle maxima. The estimate of the time of each maximum was improved using quadratic interpolation

period. Overall, the generalizability of many of our results recommends our approach as a useful starting point for the analysis of the effects of interaction structure on the appearance of asynchronous equilibria in these systems.

6 Conclusions

Through the analysis of our relatively simple multilayer oscillator model, we have illustrated the conditions underlying pattern formation on multilayer networks and provided methods for predicting the asynchronous dynamics of coupled oscillators based on their interaction structure. In particular, we highlight several mechanisms governing the appearance of asynchronous equilibria in these networks. In the first case, the phases of oscillators which are antiphase ($\theta_i - \theta_j = \pi$) do not influence each other and will cause the amplitude of both patches to decrease (Fig. 2: two cluster). In the second, oscillators with the same phase may differ in terms of amplitude if the positions of the two oscillators in the interaction structure are not isomorphic (Fig. 2: three-cluster line). Finally, an oscillator's phase may be locked if the effects of the oscillators with which it interacts are equal and opposite, or otherwise balance to zero (Fig. 2: three-cluster triangle). This mechanism has the potential to produce the most variable type and number of asynchronous dynamics while also being the most challenging to predict, as, unlike the previous mechanisms, phase locking depends also on the amplitudes of each oscillator relative to their neighbors.

Our analysis of three-oscillator systems also reveals several properties of the structure of interactions among oscillators which determine the amplitude of oscillators for asynchronous equilibria. These properties act on two scales: affecting oscillators individually and affecting the entire system uniformly. For an individual oscillator, amplitude is influenced most by strong interactions with neighbors with large differences in phase. Individual oscillators are also affected indirectly by interactions of other oscillators with its neighbors. In these cases, amplitude is affected most strongly when phase differences or interactions between a neighbor and its neighbors are small

or weak. Finally, the amplitudes of all oscillators in a system are affected equally by the total dispersal of each oscillator, the cofactors describing coupling between each pair of oscillators, and the determinant of the matrix combining the effects of interaction strength and phase difference $B = L_{ij}\cos(\theta_i - \theta_j)$. The effects on amplitude at each scale compete with one another: individual differences in amplitude among oscillators are highest when there is no system-wide effect and vice versa. These effects are also influenced by the overall strength of coupling δ and the repelling force of the limit cycle's center ψ. All effects increase with coupling strength δ; however, indirect effects and the system-wide effect on amplitude are influenced more strongly. Conversely, direct effects scale exponentially with the center's repelling force ψ, while indirect effects scale linearly and system-wide effects are not influenced. Altogether our analysis of these effects of interaction structure on oscillator amplitude provides valuable insight into the drivers of differentiation among multilayer oscillator systems during pattern formation.

Overall, the analysis of our model presents a wider view of the mechanisms underlying the formation of asynchronous patterns by investigating the effects of structure on asynchronous equilibria. Our methods can be applied to inform the design of interacting systems to minimize asynchronous pattern formation where this is desired, such as in power grids (Sachtjen et al. 2000) and wireless communication (Díaz-Guilera and Arenas 2008). Alternatively, our methods describe how the differentiating effects of asynchronous patterns can be predicted and manipulated through the structure of interactions for other applications, such as studies of brain function (Uhlhaas et al. 2010) and reserve design in ecology (Holyoak and Fahrig 2000).

Acknowledgements Kurt E. Anderson was supported in part by NSF DEB 1553718.

References

Aguiar MA, Dias APS (2014) The lattice of synchrony subspaces of a coupled cell network: characterization and computation algorithm. J Nonlinear Sci 24(6):949–996

Albert R, Barabási AL (2002) Statistical mechanics of complex networks. Rev Mod Phys 74(1):47

Arenas A, Díaz-Guilera A, Kurths J, Moreno Y, Zhou C (2008) Synchronization in complex networks. Phys Rep 469(3):93–153

Asllani M, Busiello DM, Carletti T, Fanelli D, Planchon G (2014) Turing patterns in multiplex networks. Phys Rev E 90(4):042814

Barahona M, Pecora LM (2002) Synchronization in small-world systems. Phys Rev Lett 89(5):054101

Boccaletti S, Latora V, Moreno Y, Chavez M, Hwang DU (2006) Complex networks: structure and dynamics. Phys Rep 424(4):175–308

Boccaletti S, Bianconi G, Criado R, Del Genio CI, Gómez-Gardenes J, Romance M, Sendina-Nadal I, Wang Z, Zanin M (2014) The structure and dynamics of multilayer networks. Phys Rep 544(1):1–122

Brechtel A, Gramlich P, Ritterskamp D, Drossel B, Gross T (2018) Master stability functions reveal diffusion-driven pattern formation in networks. Phys Rev E 97(3):032307

Cross MC, Hohenberg PC (1993) Pattern formation outside of equilibrium. Rev Mod Phys 65(3):851

Díaz-Guilera A, Arenas A (2008) Phase patterns of coupled oscillators with application to wireless communication. In: Bio-inspired computing and communication. Springer, pp 184–191

Do AL, Höfener J, Gross T (2012) Engineering mesoscale structures with distinct dynamical implications. New J Phys 14(11):115022

Faloutsos M, Faloutsos P, Faloutsos C (1999) On power-law relationships of the internet topology. In: ACM SIGCOMM computer communication review, vol 29. ACM, pp 251–262

Freeman LC (1996) Some antecedents of social network analysis. Connections 19(1):39–42
Goldwyn EE, Hastings A (2008) When can dispersal synchronize populations? Theor Popul Biol 73(3):395–402
Hata S, Nakao H, Mikhailov AS (2014) Dispersal-induced destabilization of metapopulations and oscillatory turing patterns in ecological networks. Sci Rep 4:3585
Hayes SM, Anderson KE (2018) Beyond connectivity: how the structure of dispersal influences metacommunity dynamics. Theor Ecol 11(2):151–159
Holland MD, Hastings A (2008) Strong effect of dispersal network structure on ecological dynamics. Nature 456(7223):792–794
Holyoak M, Fahrig L (2000) Habitat patch arrangement and metapopulation persistence of predators and prey. Am Nat 156(4):378–389
Jeong H, Tombor B, Albert R, Oltvai ZN, Barabási AL (2000) The large-scale organization of metabolic networks. Nature 407(6804):651–654
Kamei H, Cock PJ (2013) Computation of balanced equivalence relations and their lattice for a coupled cell network. SIAM J Appl Dyn Syst 12(1):352–382
Kouvaris NE, Hata S, Díaz-Guilera A (2015) Pattern formation in multiplex networks. Sci Rep 5:10840
Kuramoto Y (1975) Self-entrainment of a population of coupled non-linear oscillators. In: International symposium on mathematical problems in theoretical physics. Springer, pp 420–422
Nakao H, Mikhailov AS (2010) Turing patterns in network-organized activator-inhibitor systems. Nat Phys 6(7):544–550
Pecora LM, Carroll TL (1998) Master stability functions for synchronized coupled systems. Phys Rev Lett 80(10):2109
Rosenzweig ML, MacArthur RH (1963) Graphical representation and stability conditions of predator–prey interactions. Am Nat 97:209–223
Sachtjen M, Carreras B, Lynch V (2000) Disturbances in a power transmission system. Phys Rev E 61(5):4877
Stewart I, Golubitsky M, Pivato M (2003) Symmetry groupoids and patterns of synchrony in coupled cell networks. SIAM J Appl Dyn Syst 2(4):609–646
Strogatz SH (2000) From kuramoto to crawford: exploring the onset of synchronization in populations of coupled oscillators. Physica D 143(1):1–20
Strogatz SH (2001) Exploring complex networks. Nature 410(6825):268–276
Turing AM (1952) The chemical basis of morphogenesis. Philos Trans R Soc Lond B Biol Sci 237(641):37–72
Uhlhaas PJ, Roux F, Rodriguez E, Rotarska-Jagiela A, Singer W (2010) Neural synchrony and the development of cortical networks. Trends Cognit Sci 14(2):72–80
Varela F, Lachaux JP, Rodriguez E, Martinerie J (2001) The brainweb: phase synchronization and large-scale integration. Nat Rev Neurosci 2(4):229–239
Watts DJ, Strogatz SH (1998) Collective dynamics of 'small-world' networks. Nature 393(6684):440–442
Wolfrum M (2012) The turing bifurcation in network systems: collective patterns and single differentiated nodes. Physica D 241(16):1351–1357